Cytoplasmic dynein regulates its attachment to microtubules via nucleotide state-switched mechanosensing at multiple AAA domains

Matthew P. Nicholas[a,b], Florian Berger[c,d,e], Lu Rao[a], Sibylle Brenner[a], Carol Cho[f], and Arne Gennerich[a,1]

[a]Department of Anatomy and Structural Biology, Gruss Lipper Biophotonics Center, and [b]Medical Scientist Training Program, Albert Einstein College of Medicine, Bronx, NY 10461; [c]Theory and Bio-Systems, Max Planck Institute of Colloids and Interfaces, 14424 Potsdam, Germany; [d]Laboratory of Sensory Neuroscience, and [e]Howard Hughes Medical Institute, Rockefeller University, New York, NY 10065; and [f]Department of Biochemistry, Stanford University School of Medicine, Stanford, CA 94305

Cytoplasmic dynein is a homodimeric microtubule (MT) motor protein responsible for most MT minus-end–directed motility. Dynein contains four AAA+ ATPases (AAA: ATPase associated with various cellular activities) per motor domain (AAA1–4). The main site of ATP hydrolysis, AAA1, is the only site considered by most dynein motility models. However, it remains unclear how ATPase activity and MT binding are coordinated within and between dynein's motor domains. Using optical tweezers, we characterize the MT-binding strength of recombinant dynein monomers as a function of mechanical tension and nucleotide state. Dynein responds anisotropically to tension, binding tighter to MTs when pulled toward the MT plus end. We provide evidence that this behavior results from an asymmetrical bond that acts as a slip bond under forward tension and a slip-ideal bond under backward tension. ATP weakens MT binding and reduces bond strength anisotropy, and unexpectedly, so does ADP. Using nucleotide binding and hydrolysis mutants, we show that, although ATP exerts its effects via binding AAA1, ADP effects are mediated by AAA3. Finally, we demonstrate "gating" of AAA1 function by AAA3. When tension is absent or applied via dynein's C terminus, ATP binding to AAA1 induces MT release only if AAA3 is in the posthydrolysis state. However, when tension is applied to the linker, ATP binding to AAA3 is sufficient to "open" the gate. These results elucidate the mechanisms of dynein–MT interactions, identify regulatory roles for AAA3, and help define the interplay between mechanical tension and nucleotide state in regulating dynein motility.

cytoplasmic dynein | mechanosensing | optical tweezers | AAA+ ATPases | microtubules

Numerous eukaryotic cellular processes require motion and force generated by cytoskeletal motor proteins, among which cytoplasmic dynein (hereinafter, "dynein") is unique for its size, complexity, and versatility. As a homodimeric, divergent AAA+ ATPase (AAA: ATPase associated with various cellular activities), dynein drives the majority of microtubule (MT) minus-end–directed motility in most eukaryotes (1). The motor functions as a massive protein complex (2), but its catalytic core consists of two identical heavy chains, each with six AAA modules (AAA1–6) linked in tandem to form a ring (Fig. 1A). AAA1–4 bind nucleotides, whereas AAA5 and -6 are structural (3, 4). A ~15-nm "stalk" emerging from AAA4 (3, 4) separates the AAA modules from the MT-binding domain (MTBD). The stalk configuration influences both MT affinity and ATPase activity (5) and thereby mediates bidirectional allosteric communication between the AAA ring and the MTBD (3, 6). Finally, a ~10-nm "linker" also emerges from the ring and undergoes cyclic reorientations that generate force and displacement (7–9).

For dynein to "walk," one motor domain ("head") must remain MT-bound while the other moves (10–13), thus requiring coordination of the "internal" cycles of both heads. Dynein may use allosteric mechanosensing (possibly through the stalk) to differentiate between the leading and trailing heads, because they experience oppositely directed mechanical tension (Fig. 1A). Kinesin (14–16) and myosin (17–19) use similar mechanisms, exhibiting asymmetry in filament binding and nucleotide affinity in response to applied forces.

Recent studies suggest dynein stepping is indeed tension regulated. The farther apart its heads are spread on the MT (i.e., the greater the intramolecular tension), the shorter the dwell time before the next step and the greater the probability of the rear head advancing (12, 13). We demonstrated ATP-independent, force-induced bidirectional stepping by dynein in which the motor moves processively under the constant force of an optical trap. Less force was required to induce forward than backward movement (11). More recently, Cleary et al. showed that the lifetimes of single monomeric dynein–MT bonds depend on the direction of applied force (20). These results imply that mechanical tension contributes to control of dynein motion along the MT.

Within each of its two separate heads, the actions of dynein's multiple AAA domains may also be coordinated. Most models focus exclusively on AAA1 because it is the principal site of ATP hydrolysis (4, 7, 21–25), and ATP binding to AAA1 weakens MT affinity (4, 22). However, mutations affecting ATP binding or hydrolysis at sites other than AAA1 also have marked effects on dynein–MT binding and ATPase activity (22, 23, 25, 26). Thus, dynein mechanochemistry is complex, with AAA1–4 activities linked together in one composite, convolved cycle.

Significance

Cytoplasmic dynein is the primary minus-end–directed microtubule (MT) motor. It is unclear how dynein coordinates ATP hydrolysis and MT attachment within and between its two motor domains, each containing four AAA+ ATPases (AAA: ATPase associated with various cellular activities), AAA1–4. We characterize how mechanical tension and nucleotide states of AAA1 and AAA3 regulate dynein–MT binding. Dynein binds MTs tighter when subjected to tension opposite its normal motility. ADP binding to AAA3 unexpectedly weakens MT-binding strength and reduces the bond strength anisotropy. Finally, AAA3 "gates" the activity of AAA1: ATP binding to AAA1 induces MT release only if AAA3 contains nucleotide. This work expands understanding of the role of force in dynein mechanochemistry and identifies regulatory functions of AAA3.
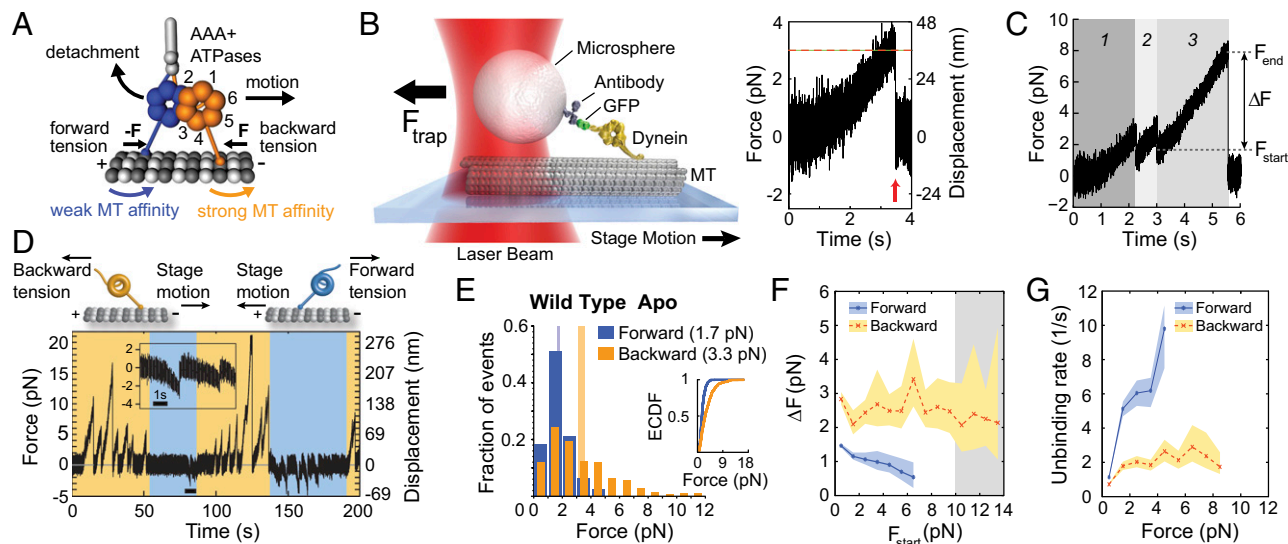
Fig. 1. Dynein–MT bond anisotropy. (*A*) Model for tension-based regulation of dynein stepping. Splaying of the dynein heads generates intramolecular tension. Under backward tension (front head) MT binding strength is greater, and under forward tension (rear head) it decreases. (*B*, *Left*) A polystyrene bead bearing a dynein motor is held in an optical trap as the microscope stage sweeps back and forth parallel to a MT (not to scale). (*Right*) The motor binds the MT, pulling the bead out of the trap. Force on the motor increases until the dynein–MT bond ruptures at the "unbinding force" (red arrow), here ~3 pN. (*C*) Primary and secondary unbinding events. Event 1 is a primary event, beginning from zero force. Secondary events (2 and 3) occur when the motor rebinds the MT before returning to the trap center. These events begin with preload F_{start} and unbind again at F_{end}, with force difference $\Delta F = F_{start} - F_{end}$. (*D*) Force (position) vs. time for WT dynein in the apo state. The inserted trace segment corresponds to the data for the period marked by the thick black line. Orange and blue shaded areas show periods of applied backward and forward tension, respectively (loading rate: 5.6 pN/s; $k \sim 0.07$ pN/nm, $v_{stage} \sim 80$ nm/s). (*E*) Normalized histograms of primary forward ($n = 575$) and backward ($n = 512$) unbinding forces, with mean values noted above the histograms. Tall vertical bands represent 95% CIs of the means (forward: [1.7, 1.8] pN, backward: [3.1, 3.6] pN) estimated by bootstrapping 4,000 samples. (*Inset*) ECDFs for the forward vs. backward directions. (*F*) Mean ΔF vs. F_{start} for forward (blue) and backward (orange) tension. Events grouped into 1-pN bins for F_{start}. Shaded regions: 95% CIs for the mean ΔF, estimated by bootstrapping 2,000 samples. For $F_{start} \gtrsim 10$ pN (gray shaded region), the trap stiffness is not constant (*SI Appendix, SI Text* and Fig. S4) and 20 or fewer events were recorded. For $F_{start} \leq 10$ pN, each mean ΔF was calculated from 36 to 770 measurements. (*G*) Unbinding rate vs. loading force derived from the data in *E* (see *SI Appendix, SI Text* for details). The shaded areas represent 95% CIs for the mean rates, estimated by bootstrapping 4,000 samples.

Here, we examine directly how tension affects dynein–MT binding and decipher how nucleotide states of AAA1 and AAA3 modulate dynein's MT attachment in the presence of force. Using an approach pioneered by the laboratory of Shin'ichi Ishiwata (14, 16), we use optical tweezers (Fig. 1*B*) to measure the force required to unbind single *Saccharomyces cerevisiae* dynein heads from MTs. We show that dynein attachment to MTs is stronger [i.e., greater force is required on average to rupture the bond (27)] under backward than under forward tension. Further, we provide evidence for unusual bonding characteristics. Protein–protein bonds are generally categorized as "slip" bonds (most common), which rupture more rapidly when force is applied; "catch" bonds (less common), which rupture more slowly in the presence of tension; and "ideal" bonds (uncommon), which are insensitive to mechanical stress (28–30). Under forward load, we find that dynein exhibits slip bonding. However [in contrast to reports of dynein catch bonding under backward load (31–33)], we find that dynein exhibits slip bonding (faster unbinding) for backward forces up to ~2 pN, and ideal bonding (constant, force-independent unbinding rate) for greater backward forces. We term this behavior "slip–ideal" bonding. Finally, we dissect AAA1- and AAA3-mediated nucleotide-induced modulation of dynein's inherent response to force, identifying (*i*) a previously undescribed weakening of MT attachment caused by ADP binding at AAA3 and (*ii*) a novel function for the linker in the AAA3-mediated "gating" of the nucleotide-dependent regulation of dynein–MT binding by AAA1. When tension is absent or applied via dynein's C terminus, ATP binding to AAA1 induces MT release only if AAA3 is in the posthydrolysis state, as described recently (9, 34). However, under more physiological conditions in which tension is applied to the linker, ATP binding to AAA3 is sufficient to "open" the regulatory gate. These results provide a basis for more complete models of the dynein mechanochemical cycle.

Results

Stronger Dynein–MT Binding Under Backward Tension.

We previously demonstrated bidirectional force-induced dynein stepping, with larger forces required to induce backward steps (toward the MT plus end) (11). We predicted this behavior results from intrinsic anisotropy of the dynein–MT bond. To define the intrinsic response of an individual dynein motor domain to force, we measured unbinding forces (Fig. 1*B*) of a tail-truncated, single-headed "wild-type" (WT) dynein (Dyn1$_{331kDa}$ or VY137 dynein; see *SI Appendix, SI Materials and Methods*) in the nucleotide-free (apo) state (Fig. 1 *C–E*), similar to Cleary et al. (20). As expected, forces required to unbind dynein monomers from MTs were significantly larger when pulling backward (Fig. 1*D*; loading rate: 5.6 pN/s). Whereas forward unbinding forces rarely exceeded 3 pN, backward unbinding forces frequently exceeded 5 pN (and rarely, beads under backward force were carried beyond the detection range of the trap, e.g., Fig. 1*D* at ~125 s).

The largest forces in both directions usually occurred after the bead repeatedly reattached to the MT before fully returning to the trap center (Fig. 1*C*). We call these "secondary" binding/unbinding events. For "primary" events, because the bead is initially positioned at the trap center, zero force is applied to the motor immediately after binding the MT ($F_{start} = 0$), whereas for secondary events $F_{start} > 0$ [referred to as a "preload" (35)]. It is difficult to compare primary and secondary unbinding forces because for a given detachment force, the history of force applied to the bond depends on F_{start}. In other words, unbinding forces must be interpreted as a function of the preload. Our initial analysis focused on primary events (zero preload).

Normalized histograms of primary unbinding forces and empirical cumulative distribution functions (ECDFs) show that, although unbinding in either direction most often occurs between 1 and 2 pN, backward unbinding forces are frequently greater (Fig. 1*E*).

Nicholas et al.

Comparison of ECDFs with a two-sample Kolmogorov–Smirnov (KS) test (36) yields a P value $p_{ks} < 10^{-10}$ (null hypothesis: the histograms have identical underlying distributions) with KS statistic $D = 0.37$ (D ranges [0,1] and measures the maximal difference between two ECDFs; see ref. 36). Although the distributions are non-Gaussian, we characterize them by the mean with 95% confidence interval for convenience (1.7 [1.7, 1.8] pN forward vs. 3.3 [3.1, 3.6] pN backward) and estimate the P value for the difference of the means via bootstrapping, $p_m < 10^{-5}$ (*SI Appendix, SI Text,* Fig. S2 for summaries of data from all experiments). Interestingly, results were similar for WT dynein with GFP at the C terminus instead of the linker (*SI Appendix, SI Text* and Fig. S3*A*).

Dynein Exhibits Slip–Ideal Bonding Under Backward Load. Under backward tension, secondary binding often results in prolonged MT attachment, even with increasing force during sequential MT encounters (Fig. 1*C*). This behavior is inconsistent with slip bonding. The higher F_{start}, the more rapidly a slip bond will break, and thus the average additional force attained ΔF will monotonically decrease. Given reports that dynein catch bonds MTs (31–33) such that the unbinding rate decreases with applied force (37, 38), we wondered whether prolonged MT attachment at high force might indicate increased bond lifetime with increasing load. Thus, we reasoned that ΔF might not decrease as a function of F_{start}.

To test this hypothesis, we measured ΔF for events with similar preloads (F_{start} bin size of 1 pN) and plotted the mean ΔF vs. F_{start} (Fig. 1*F*). Within experimental uncertainty, the mean ΔF decreases monotonically under forward load (consistent with slip bonding). However, for backward load, there is not a marked decrease, i.e., the bond breaks after a similar time (proportional to ΔF), regardless of applied force. Analysis of force-dependent unbinding rates calculated from primary unbinding events (*SI Appendix, SI Text*) (39) yielded similar results: forward unbinding rate increases with increasing load (slip bonding), but backward unbinding rate increases only up to ~2 pN and remains relatively constant as greater forces are applied (slip–ideal bonding, Fig. 1*G*).

ATP Binding to AAA1 Weakens MT Binding Under Tension. To better understand how dynein–MT binding is regulated, we next examined how nucleotide state affects dynein's response to tension. We first added saturating ATP [1 mM, predicted to induce MT release (40)]. Both forward and backward unbinding shifted toward smaller forces (Fig. 2*A*; *SI Appendix, SI Text* and Table S1) with the most notable difference in the first 1-pN bin. Preventing ATP binding with a K/A mutation in the AAA1 Walker-A motif yielded unbinding force distributions statistically indistinguishable from the WT apo state (Figs. 1*E* and 2*B*; *SI Appendix, SI Text,* Fig. S5*A*, and Table S1). Interestingly, although apo-state behavior is similar when tension is applied via dynein's C terminus rather than the linker (Fig. 1*E*; *SI Appendix, SI Text,* Fig. S3*A*), ATP weakens the dynein–MT binding strength more in the presence of C-terminal tension (Figs. 2*A* and 3*A*).

Because ATP is known to markedly diminish dynein's affinity for MTs (e.g., ref. 40), we postulated that its relatively small effect on WT unbinding forces with linker-applied tension was due to AAA1 hydrolyzing ATP, thus preventing observation of a pure ATP-bound state (*SI Appendix, SI Text,* and Fig. S6, state 1). We therefore introduced an E/Q mutation in the AAA1 Walker B motif to prevent ATP hydrolysis by AAA1. This mutant showed markedly weaker unbinding forces (mean <1 pN) in both directions in the presence of ATP compared with the apo state (Fig. 2 *C* and *D*; *SI Appendix, SI Text,* Fig. S5*B*, and Table S1). On the other hand, in AAA3, E/Q mutation yielded unbinding-force distributions similar to WT (Fig. 2 *A* and *E*). In the backward direction, there was no significant difference between the apo and ATP states (Fig. 2*E*; *SI Appendix, SI Text,* Fig. S5*C*, and Table S1), whereas forward unbinding forces for the two states exhibited a statistically significant but small difference in the mean (apo 1.5 [1.4, 1.6] pN vs. ATP 1.3 [1.2, 1.4] pN, $p_m = 0.02$).

AAA3 Regulates ATP-Induced, AAA1-Mediated MT Release. Having determined that AAA1 mediates ATP-induced MT release, we wondered whether AAA3 regulates this process. Using a AAA1 E/Q + AAA3 E/Q double mutant in the presence of 1 mM ATP, we tested whether simultaneous ATP states in AAA1 and AAA3 resulted in different behavior from an ATP state only in AAA1. This mutant behaved similarly to AAA1 E/Q in the presence of ATP (Fig. 2 *D* and *F*; *SI Appendix, SI Text* and Table S1), with
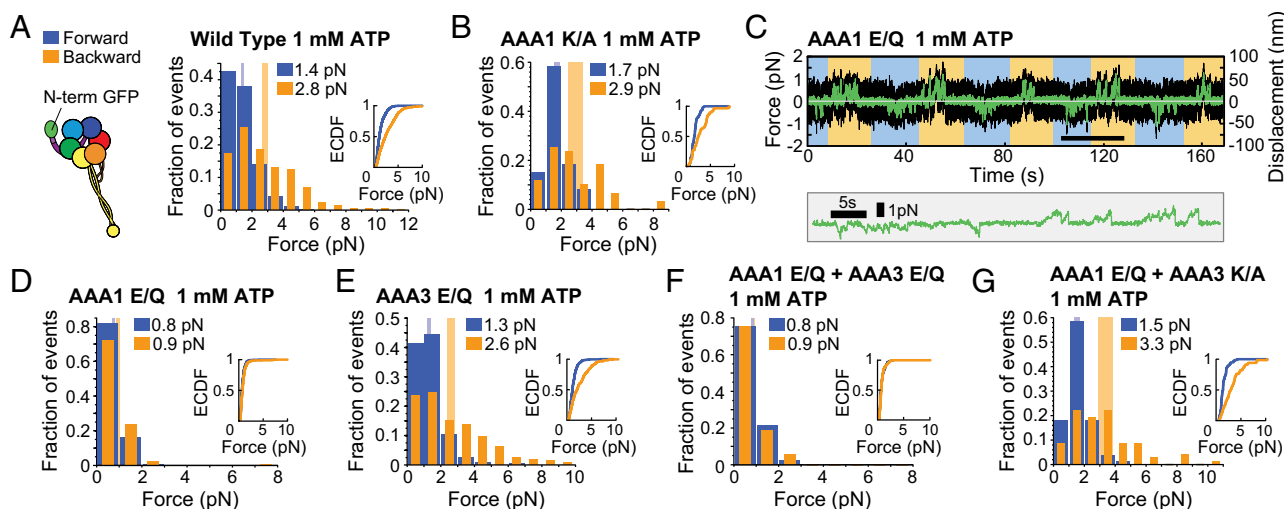
Fig. 2. Effect of 1 mM ATP on dynein's response to linker-applied tension. (*A, Left*) Schematic of dynein with GFP fused to the N terminus. (*Right*) WT dynein forward and backward unbinding forces with mean values noted. Tall vertical bands represent 95% CIs of the means (forward: [1.4, 1.5] pN, backward: [2.6, 2.9] pN) estimated by bootstrapping 4,000 samples. (*B*) As in *A*, but for the AAA1 K/A mutant (95% CIs [1.5, 1.9] and [2.5, 3.4] pN). (*C*) Example of optical trapping data for the AAA1 E/Q mutant. Black trace shows raw data. Green trace shows a fifth-order Savitzky–Golay filter with a 301-sample (0.1-s) window applied to the data to make unbinding events easier to identify. The detail shows the filtered data for the period marked by the thick black line. (*D*) As in *A*, but for the AAA1 E/Q mutant (95% CIs [0.7, 0.8] and [0.9, 1.0] pN). (*E*) As in *A*, but for the AAA3 E/Q mutant (95% CIs [1.2, 1.4] and [2.4, 2.8] pN). (*F*) As in *A*, but for the AAA1 E/Q + AAA3 E/Q mutant (95% CIs [0.8, 0.9] and [0.8, 0.9] pN). (*G*) As in *A*, but for the AAA1 E/Q + AAA3 K/A mutant (95% CIs [1.4, 1.7] and [2.9, 3.8] pN). Number of events in the forward, backward directions: (*A*) (577, 577), (*B*) (60, 59), (*D*) (320, 365), (*E*) (272, 294), (*F*) (274, 292), and (*G*) (77, 67).
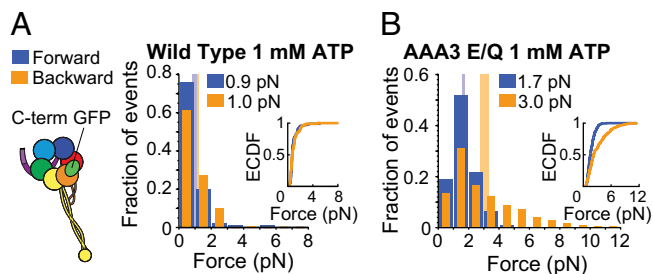
Nicholas et al.

Fig. 3. Primary unbinding forces for the WT (*A*) and the AAA3 E/Q mutant (*B*) with GFP fused to the C terminus in the presence of 1 mM ATP. Tension is applied via the C terminus (loading rate: 5.6 pN/s). (*A, Left*) Schematic of dynein with GFP fused to the C terminus. (*Right*) Histogram of WT dynein forward (blue) and backward (orange) unbinding forces, with the respective mean values noted above each histogram. Tall vertical bands represent 95% CIs of the means (forward: [0.8, 1.1] pN, backward: [0.9, 1.2] pN) estimated by bootstrapping 4,000 samples. (*B*) As in *A*, but for the AAA3 E/Q mutant (95% CIs [1.6, 1.8] and [2.7, 3.3] pN). Number of events in the forward, backward directions: (*A*) (95, 98) and (*B*) (228, 229).

marked weakening of MT-binding strength versus the apo state (Fig. 2*F*; *SI Appendix, SI Text*, Fig. S5*D*, and Table S1). In contrast, when we prevented ATP binding to AAA3 in an AAA1 E/Q + AAA3 K/A double mutant, ATP no longer caused significant weakening of MT-binding strength (Fig. 2*G*; *SI Appendix, SI Text, Fig. S5E, and Table S1*) and instead yielded behavior similar to AAA1 K/A (Fig. 2*B*; *SI Appendix, SI Text* and Table S1).

The Site of Applied Tension Modifies AAA1 Gating by AAA3. As mentioned above, WT unbinding forces were markedly weakened by addition of ATP in the presence of C terminal, but not linker-applied tension. We wondered whether the site of applied tension also affects the AAA3-based gating of AAA1. Recent work by DeWitt et al. (zero-load studies and optical trapping with C-terminal tension) (34) and Bhabha et al. (zero-load studies) (9) reported similar AAA3-based regulation, but concluded that AAA3 must be in the post-ATP hydrolysis state to allow MT release. We also found that under C-terminal tension, the AAA3 E/Q mutant no longer showed ATP-induced weakened MT binding (Fig. 3 *A* and *B*; *SI Appendix, SI Text*, Fig. S3*B*, and Table S1). In addition, both the N- and C-terminal GFP-tagged AAA3 E/Q mutants showed insignificant release from MTs upon the addition of ATP in our "zero-load" MT binding and release (MTBR) assay, in contrast to the N- and C-terminal GFP-tagged WT motors (*SI Appendix, SI Text* and Fig. S7). However, under linker-applied tension, we found that ATP does weaken MT binding of the AAA3 E/Q mutant and of the AAA1 E/Q + AAA3 E/Q double mutant (Fig. 2 *A* and *D–F*).

ADP Binding to AAA1 Strengthens MT Binding, Whereas ADP Binding to AAA3 Weakens It. Having explored the response to tension and nucleotide in the apo and ATP states, we next determined the effects of ADP (*SI Appendix, SI Text* and Fig. S6, states 4 and 5). In biochemical studies, *Dictyostelium* dynein–MT affinity is the same in the apo (*SI Appendix, SI Text* and Fig. S6, state 6) and ADP states (*SI Appendix, SI Text* and Fig. S6, state 5, postpowerstroke) (40). We thus expected similar unbinding forces in apo vs. ADP states. Surprisingly, ADP (2 or 5 mM) reduced unbinding forces in both directions and minimized the intrinsic unbinding force anisotropy of the apo state (Figs. 1*E* and 4 *A* and *B*; *SI Appendix, SI Text*, Fig. S8 *A–C*, and Table S1).

To test whether the unexpected effect of ADP was due to ADP binding AAA1, we used the AAA1 K/A mutant. A total of 2 mM ADP significantly decreased unbinding forces in both directions (Figs. 4*C* and 5; *SI Appendix, SI Text*, Fig. S5*A*, and Table S1). In fact, whereas the apo state unbinding force histograms for the WT and AAA1 K/A mutants were statistically indistinguishable (*SI Appendix, SI Text* and Table S1), ADP addition to the AAA1 K/A mutant yielded mean forces even smaller than those of the WT

($p_m < 10^{-5}$ for both directions). To examine the effect of ADP binding to AAA3, we made an AAA3 K/A mutant. Apo- and (2 mM) ADP-state forward unbinding forces were statistically indistinguishable (Fig. 4*D*; *SI Appendix, SI Text, Fig. S5F, and Table S1*, $p_{ks} = 0.67$). Although the backward unbinding force histograms were also qualitatively similar (Fig. 4*D*; *SI Appendix, SI Text* and Fig. S5*F*), the mean backward unbinding force was greater in the ADP state (ADP 3.8 [3.5, 4.1] pN vs. apo 3.0 [2.7, 3.4] pN; *SI Appendix, SI Text* and Table S1, $p_{ks} = 0.017$, $p_m = 0.001$).

Discussion

Anisotropy of Dynein–MT Binding and the Response to Force. Our results are consistent with our own (11) and others' reports (12, 13, 20) that less force is required to break the dynein–MT bond when pulling the motor forward than backward. Interestingly, in the apo state, whether tension is applied via the linker vs. the C terminus has little effect on unbinding forces, implying that linker conformation and/or tension transmitted through the dynein ring are not responsible for the anisotropy. Cleary et al. observed similar results for a stalk/MTBD construct lacking the entire dynein ring (20). The molecular mechanism for the anisotropy remains to be elucidated and could include tension-induced reconfiguration of the coiled-coil stalk [which allosterically regulates MT affinity (5, 41, 42)], direct force-induced changes in the MTBD, geometrical reorientations of the binding interface, or even strain-induced effects on the MT lattice (43).

By deriving force-dependent detachment rates from primary unbinding forces, we found slip bonding by dynein to the MT under forward load. Under backward load, catch bonding (diminished unbinding rate with applied force) has been reported (31–33), but we instead found that slip bonding occurs up to ~2 pN, above which the unbinding rate is insensitive to force (Fig. 1 *F* and *G*), characteristic of ideal bonding (these findings agree with those from constant-force assays (20) that directly measure unbinding rates). Because the behavior seen here under rearward force exhibits features of both slip bonding (at low force) and ideal bonding (at higher force), we term it slip–ideal bonding. The
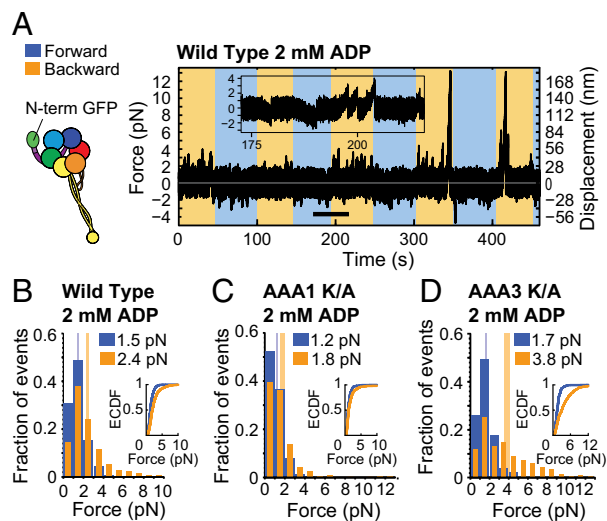

Fig. 4. Effect of ADP on dynein's response to linker-applied tension. (*A, Left*) Schematic of dynein with GFP fused to the N terminus. (*Right*) Optical trapping data. The inserted trace segment corresponds to data for the period marked by the thick black line. (*B*) Histogram of WT dynein forward (blue) and backward (orange) unbinding forces measured in the presence of 2 mM ADP, with the respective mean values noted above each histogram. Tall vertical bands represent 95% CIs of the means (forward: [1.4, 1.5] pN, backward: [2.3, 2.5] pN. (*C*) As in *B*, but for the AAA1 K/A mutant (95% CIs [1.1, 1.3] and [1.6, 2.0] pN). (*D*) As in *B*, but for the AAA3 K/A mutant (95% CIs [1.6, 1.8] and [3.5, 4.1] pN). Number of events in the forward, backward directions: (*B*) (996, 869), (*C*) (325, 387), and (*D*) (439, 369).
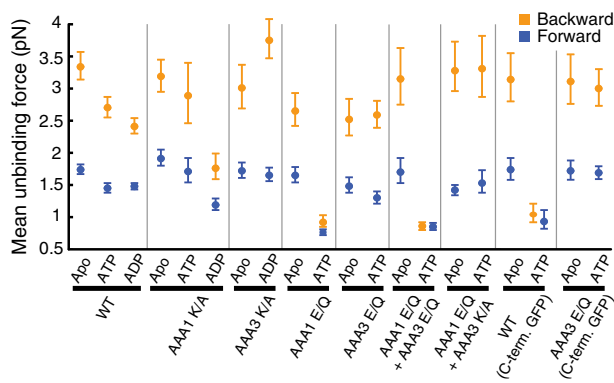
Nicholas et al.

www.manaraa.com

Fig. 5. Mean forward (blue) and backward (orange) unbinding forces for the various experiments reported. Error bars denote 95% CIs of the mean. The labels on the abscissa denote the experimental condition tested (*Top* row) and the constructs used (*Bottom* row).

underlying mechanism is unclear; to our knowledge this is the first report of such behavior. In a physiological context, ideal bonding may allow dynein to maintain its attachment to MTs in the presence of large opposing loads, whereas the pure slip-bonding and lesser binding strength in the forward direction may allow the motor to be pulled forward by other dyneins when working as part of a team pulling a single cargo.

Differential Effects of ADP and ATP at AAA1 and Evidence for Tension-Controlled Nucleotide Affinity. Whereas the AAA1 K/A mutant in the presence of ADP binds MTs more weakly than WT under forward and backward load (Fig. 4 *B* and *C*), the AAA3 K/A mutant binds MTs more strongly under backward load with ADP than in the apo state (Fig. 4*D*; *SI Appendix, SI Text* and Fig. S5*F*). These results suggest that, whereas ADP binding to AAA3 weakens the dynein–MT bond (discussed below), ADP at AAA1 strengthens it (consistent with the assumption that AAA1 retains ADP as dynein assumes postpowerstroke/leading/load-bearing configurations). In contrast, ATP binding to AAA1 markedly weakens MT attachment. However, whereas AAA1 E/Q exhibits weak binding in the presence of ATP, the WT shows a significant but smaller reduction in MT bond strength. Cleary et al. recently suggested that ATP has no effect on the WT dynein force-dependent unbinding rate when pulling on the linker (20). Our results generally support this conclusion (ATP weakens MT attachment substantially with tension applied via the C terminus, but not linker). However, Cleary et al. did not report unbinding rates for forces <1 pN, the force range in which greater unbinding rates would be expected, given the increased frequency of unbinding in the first 1-pN bin of our histogram (Fig. 2*A*; *SI Appendix, SI Text* and Fig. S9 *A–C*). Indeed, the WT apo and ATP unbinding rates in both directions are statistically indistinguishable for forces of 1–8 pN (*SI Appendix, SI Text* and Fig. S9*D*). Thus, for tension applied via the linker, ATP has a significant effect only for small forces ($\lesssim 1$ pN).

Dynein behavior in the absence and presence of ATP could converge if tension reduces dynein's ATP affinity, explaining the similar behaviors observed for forces >1 pN (see *SI Appendix, SI Text* for detailed discussion). This would imply tension "gates" ATP binding to AAA1. Because dynein–MT binding strength is greater under backward tension, this gating mechanism would help regulate stepping by working synergistically with the intrinsic anisotropy of the dynein–MT bond strength. Backward tension on the front head leads to stronger MT binding, thereby "anchoring" the head in place. This same tension could simultaneously block ATP binding/hydrolysis in the front head until relief of intramolecular tension by release of the trailing head. Future studies should address how tension affects AAA1 ATP affinity.

Nicholas et al.

Gating of AAA1-Mediated, ATP-Induced MT Release by AAA3. Although AAA3 plays an important role in controlling dynein–MT attachment (22, 23, 25), the details are just emerging. By probing dynein–MT interactions in the absence of load (9, 34) and with force applied to the dynein C terminus (34), DeWitt et al. and Bhabha et al. concluded that AAA3 must be in a posthydrolysis state for ATP-induced, AAA1-mediated MT release. Our MTBR and C-terminal pulling results support these findings, but if tension is applied via the linker, then AAA1-mediated MT release is allowed when AAA3 enters the ATP state.

It is unclear how AAA3 gates AAA1 function and how linker- vs. C-terminal tension alters this regulation. However, recent reports relate linker conformation to dynein's ATPase activities. In the absence of load, ATP at AAA3 blocks reorientation of the linker from the post- to the prepowerstroke conformation (9). In addition, binding of the cofactor Lis1, which mechanically obstructs linker movements, uncouples AAA1's ATPase activities from changes in MT-binding affinity (44). Finally, AAA5 mutations preventing linker docking severely reduce dynein's ATPase activities (3, 8). Thus, tension-induced changes in linker conformation could allosterically regulate AAA3 nucleotide state and/or AAA3–AAA1 communication, and thereby alter the effects of specific nucleotide states on AAA3-based gating of AAA1 function. This is the first evidence to our knowledge that tension applied via the linker modulates AAA3–AAA1 communication.

Weakening of MT-Binding Induced by ADP at AAA3. Somewhat unexpectedly, ADP binding to AAA3 weakens MT binding and minimizes the asymmetry between forward and backward unbinding forces (Figs. 1*E* and 4; *SI Appendix, SI Text* and Fig. S8). In the absence of force, *Dictyostelium* dynein binds MTs with essentially equal affinities in the apo and ADP states (40). However, recent yeast (apo) and *Dictyostelium* (ADP-bound) dynein crystal structures suggest that ADP release causes rearrangements within the motor domain (45). In particular, reorientations of the buttress and AAA6L/AAA5S relative to the stalk and AAA5S/AAA4S (*SI Appendix, SI Text* and Fig. S1*C*) could induce reconfigurations of the stalk and MTBD, resulting in weak MT binding. However, the apparent rearrangements could also be due to structural differences between yeast and *Dictyostelium* dynein. In addition, the AAA3 conformation itself is remarkably similar in both the apo and ADP-bound structures, raising the question of how ADP binding to AAA3 might physically exert its effects.

According to current models, the (AAA1) ADP state occurs immediately after the head steps forward, rebinds the MT, and performs the powerstroke. This configuration is expected to bear force, and thus it is surprising that MT binding would be weakened. Dynein may simply "tolerate" the moderate reduction in MT binding strength when ADP is bound. In vivo, load-sharing between groups of dyneins (46) may compensate for transiently weak attachment by single motors. Alternatively, the ADP state may be short-lived, e.g., tension could accelerate ADP release from AAA3 under physiological conditions. Even in the presence of ADP, the motor occasionally exhibits "apo-like" large secondary bindings/unbindings (Fig. 4*A*), perhaps due to ADP ejection from AAA3 when strain is applied. Unbinding assays similar to ours have shown that tension alters the affinity of myosins V and VI for ADP (18).

In the context of the mechanochemical cycle, perhaps the simplest explanation for the effects of ADP is that, unlike AAA1, AAA3 may not contain ADP following the powerstroke. AAA1 activity appears not to be strictly synchronized to that of the other AAA domains (4, 10, 25) and AAA3 hydrolyzes ATP an order of magnitude slower than AAA1 (34). Thus, AAA3 may be ADP bound only at "appropriate" points in the cycle, such as when the head is detached from the MT or when the rear head AAA1 binds ATP (thereby assisting in MT release).

Materials and Methods

Yeast Strains and Protein Purification. Engineering of yeast strains and protein purification were performed as described previously (10) with minor modifications (see *SI Appendix, SI Text*). Following initial purification, all constructs

except VY874 (AAA1 K/A), VY696 (AAA3 E/Q), and GY36 (AAA3 E/Q with a C-terminal GFP), which are insensitive to ATP-induced MT release (*SI Appendix, SI Text* and Fig. S7), were further purified by MT cosedimentation and ATP-induced release to isolate motors responsive to nucleotide. All protein was flash frozen in liquid nitrogen immediately after purification and stored at −80 °C. All motors contain an N-terminal GFP, except for VY219 (WT) and GY36, which have a GFP following the dynein C terminus. Yeast strains are listed in *SI Appendix, SI Text* and Table S2.

Unbinding-Force Measurement. MTs marked with bright fluorescent minus ends (*SI Appendix, SI Text* and Fig. S10) were covalently attached to glass coverslips of microscopy chambers as previously described (47). Anti-GFP antibody-coated, 1-μm diameter beads were then incubated with appropriate concentrations of dynein to produce MT binding by ≤50% of beads in the final assay, implying binding by single motors (48) (*SI Appendix, SI Text* and Fig. S11) for additional information). The assay buffer (11) contained 30 mM Hepes (pH 7.2), 2 mM Mg(Acetate)$_2$, and 1 mM EGTA, supplemented with 1 mg/mL β-casein, 10 μM paclitaxel, 10 mM DTT, and an oxygen scavenger system (49). Apyrase (6.6 units/mL) was added to deplete nucleotides in apo-state experiments, whereas ATP (1 mM) or ADP (2 mM, plus hexokinase) were added for experiments testing the effects of these nucleotides. Using optical tweezers described previously (50), beads were held over surface-bound MTs while the stage holding the slide chamber was swept in a triangle-wave pattern along the direction parallel to the MT long axis. The speed of movement was adjusted to produce a loading rate of 5.6 pN/s once

a motor bound. For data acquisition, signals were electronically low-pass filtered at 1.5 kHz and data were sampled at 3 kHz. See *SI Appendix, SI Text* for detailed protocols.

Data Analysis. Unbinding forces were measured using a semiautomated detection program written in MATLAB (see *SI Appendix, SI Text*). Measurements from multiple beads and experiments under the same conditions were pooled together and used to generate unbinding force histograms with 1-pN bins. The 95% confidence intervals (CIs) of the mean were calculated by bootstrapping. ECDFs for unbinding forces and KS tests to compare distributions were calculated using built-in MATLAB functions. Calculation of P values when comparing sample means was also done using bootstrapping. See *SI Appendix, SI Text* for detailed protocols.

1. Vallee RB, McKenney RJ, Ori-McKenney KM (2012) Multiple modes of cytoplasmic dynein regulation. *Nat Cell Biol* 14(3):224–230.
2. Kardon JR, Vale RD (2009) Regulators of the cytoplasmic dynein motor. *Nat Rev Mol Cell Biol* 10(12):854–865.
3. Schmidt H, Gleave ES, Carter AP (2012) Insights into dynein motor domain function from a 3.3-Å crystal structure. *Nat Struct Mol Biol* 19(5):492–497, S1.
4. Kon T, et al. (2012) The 2.8 Å crystal structure of the dynein motor domain. *Nature* 484(7394):345–350.
5. Kon T, et al. (2009) Helix sliding in the stalk coiled coil of dynein couples ATPase and microtubule binding. *Nat Struct Mol Biol* 16(3):325–333.
6. Gibbons IR, et al. (2005) The affinity of the dynein microtubule-binding domain is modulated by the conformation of its coiled-coil stalk. *J Biol Chem* 280(25):23960–23965.
7. Kon T, Mogami T, Ohkura R, Nishiura M, Sutoh K (2005) ATP hydrolysis cycle-dependent tail motions in cytoplasmic dynein. *Nat Struct Mol Biol* 12(6):513–519.
8. Toropova K, et al. (2014) Lis1 regulates dynein by sterically blocking its mechano-chemical cycle. *eLife* 3:e02641.
9. Bhabha G, et al. (2014) Allosteric communication in the dynein motor domain. *Cell* 159(4):857–868.
10. Reck-Peterson SL, et al. (2006) Single-molecule analysis of dynein processivity and stepping behavior. *Cell* 126(2):335–348.
11. Gennerich A, Carter AP, Reck-Peterson SL, Vale RD (2007) Force-induced bidirectional stepping of cytoplasmic dynein. *Cell* 131(5):952–965.
12. DeWitt MA, Chang AY, Combs PA, Yildiz A (2012) Cytoplasmic dynein moves through uncoordinated stepping of the AAA+ ring domains. *Science* 335(6065):221–225.
13. Qiu W, et al. (2012) Dynein achieves processive motion using both stochastic and coordinated stepping. *Nat Struct Mol Biol* 19(2):193–200.
14. Uemura S, et al. (2002) Kinesin-microtubule binding depends on both nucleotide state and loading direction. *Proc Natl Acad Sci USA* 99(9):5977–5981.
15. Yildiz A, Tomishige M, Gennerich A, Vale RD (2008) Intramolecular strain coordinates kinesin stepping behavior along microtubules. *Cell* 134(6):1030–1041.
16. Uemura S, Ishiwata S (2003) Loading direction regulates the affinity of ADP for kinesin. *Nat Struct Biol* 10(4):308–311.
17. Gebhardt JCM, Clemen AE-M, Jaud J, Rief M (2006) Myosin-V is a mechanical ratchet. *Proc Natl Acad Sci USA* 103(23):8680–8685.
18. Oguchi Y, et al. (2008) Load-dependent ADP binding to myosins V and VI: Implications for subunit coordination and function. *Proc Natl Acad Sci USA* 105(22):7714–7719.
19. Dunn AR, Chuan P, Bryant Z, Spudich JA (2010) Contribution of the myosin VI tail domain to processive stepping and intramolecular tension sensing. *Proc Natl Acad Sci USA* 107(17):7746–7750.
20. Cleary FB, et al. (2014) Tension on the linker gates the ATP-dependent release of dynein from microtubules. *Nat Commun* 5:4587.
21. Gibbons IR, et al. (1987) Photosensitized cleavage of dynein heavy chains. Cleavage at the "V1 site" by irradiation at 365 nm in the presence of ATP and vanadate. *J Biol Chem* 262(6):2780–2786.
22. Silvanovich A, Li MG, Serr M, Mische S, Hays TS (2003) The third P-loop domain in cytoplasmic dynein heavy chain is essential for dynein motor function and ATP-sensitive microtubule binding. *Mol Biol Cell* 14(3):1355–1365.
23. Kon T, Nishiura M, Ohkura R, Toyoshima YY, Sutoh K (2004) Distinct functions of nucleotide-binding/hydrolysis sites in the four AAA modules of cytoplasmic dynein. *Biochemistry* 43(35):11266–11274.
24. Takahashi Y, Edamatsu M, Toyoshima YY (2004) Multiple ATP-hydrolyzing sites that potentially function in cytoplasmic dynein. *Proc Natl Acad Sci USA* 101(35):12865–12869.
25. Cho C, Reck-Peterson SL, Vale RD (2008) Regulatory ATPase sites of cytoplasmic dynein affect processivity and force generation. *J Biol Chem* 283(38):25839–25845.
26. Reck-Peterson SL, Vale RD (2004) Molecular dissection of the roles of nucleotide binding and hydrolysis in dynein's AAA domains in Saccharomyces cerevisiae. *Proc Natl Acad Sci USA* 101(6):1491–1495.
27. Evans E, Ritchie K (1997) Dynamic strength of molecular adhesion bonds. *Biophys J* 72(4):1541–1555.
28. Rakshit S, Zhang Y, Manibog K, Shafraz O, Sivasankar S (2012) Ideal, catch, and slip bonds in cadherin adhesion. *Proc Natl Acad Sci USA* 109(46):18815–18820.
29. Dembo M (1994) On peeling an adherent cell from a surface. *Lectures on Mathematics in the Life Sciences, Some Mathematical Problems in Biology* (American Mathematical Society, Providence, RI) Vol 24, pp 51–77.
30. Evans E (2001) Probing the relation between force—lifetime—and chemistry in single molecular bonds. *Annu Rev Biophys Biomol Struct* 30:105–128.
31. Kunwar A, et al. (2011) Mechanical stochastic tug-of-war models cannot explain bidirectional lipid-droplet transport. *Proc Natl Acad Sci USA* 108(47):18960–18965.
32. Leidel C, Longoria RA, Gutierrez FM, Shubeita GT (2012) Measuring molecular motor forces in vivo: Implications for tug-of-war models of bidirectional transport. *Biophys J* 103(3):492–500.
33. Rai AK, Rai A, Ramaiya AJ, Jha R, Mallik R (2013) Molecular adaptations allow dynein to generate large collective forces inside cells. *Cell* 152(1-2):172–182.
34. DeWitt MA, Cypranowska CA, Cleary FB, Belyy V, Yildiz A (2015) The AAA3 domain of cytoplasmic dynein acts as a switch to facilitate microtubule release. *Nat Struct Mol Biol* 22(1):73–80.
35. Yakovenko O, et al. (2008) FimH forms catch bonds that are enhanced by mechanical force due to allosteric regulation. *J Biol Chem* 283(17):11596–11605.
36. Conover WJ (1999) *Practical Nonparametric Statistics* (Wiley, New York), 3rd Ed.
37. Thomas W (2008) Catch bonds in adhesion. *Annu Rev Biomed Eng* 10:39–57.
38. Thomas WE, Vogel V, Sokurenko E (2008) Biophysics of catch bonds. *Annu Rev Biophys* 37:399–416.
39. Dudko OK, Hummer G, Szabo A (2008) Theory, analysis, and interpretation of single-molecule force spectroscopy experiments. *Proc Natl Acad Sci USA* 105(41):15755–15760.
40. Imamula K, Kon T, Ohkura R, Sutoh K (2007) The coordination of cyclic microtubule association/dissociation and tail swing of cytoplasmic dynein. *Proc Natl Acad Sci USA* 104(41):16134–16139.
41. Carter AP, et al. (2008) Structure and functional role of dynein's microtubule-binding domain. *Science* 322(5908):1691–1695.
42. Redwine WB, et al. (2012) Structural basis for microtubule binding and release by dynein. *Science* 337(6101):1532–1536.
43. Krebs A, Goldie KN, Hoenger A (2004) Complex formation with kinesin motor domains affects the structure of microtubules. *J Mol Biol* 335(1):139–153.
44. Huang J, Roberts AJ, Leschziner AE, Reck-Peterson SL (2012) Lis1 acts as a "clutch" between the ATPase and microtubule-binding domains of the dynein motor. *Cell* 150(5):975–986.
45. Carter AP (2013) Crystal clear insights into how the dynein motor moves. *J Cell Sci* 126(Pt 3):705–713.
46. Holzbaur ELF, Goldman YE (2010) Coordination of molecular motors: From in vitro assays to intracellular dynamics. *Curr Opin Cell Biol* 22(1):4–13.
47. Nicholas MP, Rao L, Gennerich A (2014) Covalent immobilization of microtubules on glass surfaces for molecular motor force measurements and other single-molecule assays. *Methods Mol Biol* 1136:137–169.
48. Gutiérrez-Medina B, Fehr AN, Block SM (2009) Direct measurements of kinesin torsional properties reveal flexible domains and occasional stalk reversals during stepping. *Proc Natl Acad Sci USA* 106(40):17007–17012.
49. Swoboda M, et al. (2012) Enzymatic oxygen scavenging for photostability without pH drop in single-molecule experiments. *ACS Nano* 6(7):6364–6369.
50. Nicholas MP, Rao L, Gennerich A (2014) An improved optical tweezers assay for measuring the force generation of single kinesin molecules. *Methods Mol Biol* 1136:171–246.

www.manaraa.com